MR Imaging of Neurodegeneration

11

Tammie L. S. Benzinger and Saurabh Jindal

Key Points

- Recent innovations in MR imaging allow not only to rule out organic dementia but also to differentiate various dementia subtypes and quantify the atrophic changes.
- The use of advanced imaging biomarkers such as volumetric, functional, and diffusion MRI provides early detection of neurodegeneration impacting disease management.

Introduction

The prevalence of neurodegenerative diseases is increasing with the increase in the aging population. Alzheimer's disease (AD) is the most common neurodegenerative disorder estimated to globally impact 67 million individuals by the year 2030, respectively [1]. Neuroimaging serves as a noninvasive tool to investigate the structural and functional aspects of the brain. Magnetic resonance imaging (MRI) is the first line modality in the workup of patients with slowly progressive dementia [2]. It allows for qualitative and quantitative detection of changes. It also aids in the tracking of disease progression. In this chapter, we will discuss the application of structural and functional MRI techniques in various dementia subtypes.

T. L. S. Benzinger (✉)
Neuroradiology Section, Department of Radiology, Mallinckrodt Institute of Radiology, Washington University in St. Louis, Saint Louis, MO, USA
e-mail: benzingert@wustl.edu

S. Jindal
Neuroimaging Laboratories-Research Center, Mallinckrodt Institute of Radiology, Washington University in St. Louis, Saint Louis, MO, USA
e-mail: jindals@wustl.edu

Structural Imaging

Protocol Considerations

A standardized imaging protocol optimized to detect dementia-related changes is essential. A magnetic field strength of ≥1.5Tesla (T) is required to appreciate subtle volume changes. A good quality structural MRI requires a high signal-to-noise ratio (SNR). Three-dimensional (3D) T1-weighted imaging (WI) with 256 mm field of view and ≤ 1.2 × 1.2 × 1.2 mm resolution offers high spatial resolution and is best for morphometric images [3]. Magnetization prepared rapid acquisition echo (MPRAGE) (Siemens), spoiled gradient recalled sequence (SPGR) (General Electronic), and 3D turbo field echo (Philips) are the most commonly used sequences. The rest of the protocol can be tailored based on the setting whether clinical or research. In clinical practice, two-dimensional (2D) fluid-attenuated inversion recovery (FLAIR) and 2D gradient recall echo/susceptibility weighted

© The Author(s), under exclusive license to Springer Nature Switzerland AG 2023

D. J. Cross et al. (eds.), *Molecular Imaging of Neurodegenerative Disorders*,
https://doi.org/10.1007/978-3-031-35098-6_11

imaging (GRE/SWI) are generally obtained. A 2D T2-WI, diffusion weighted imaging (DWI), post-contrast imaging, and magnetic resonance angiography are optional depending on the suspected etiology and availability of time [3]. Suggested guidelines for image acquisition of these sequences is available from the American College of Radiology [4]. For research purposes, 1 mm thick sagittal 3D FLAIR, 3 mm thick 3D GRE/SWI, resting-state functional MRI (rsfMRI) with a repetition time (TR) of 2000 ms, and diffusion tensor imaging (DTI) having ≥30 directions may be acquired with optional arterial spin labeling (ASL) images [3]. The Alzheimer's Disease Neuroimaging Initiative (ADNI) has published guidelines for performance of MRI for dementias and is a useful resource [5]. Protocol for serial longitudinal scans should be consistent for accurate follow-up. In particular, if assessing for serial microbleeds or siderosis, consistent field strength and choice of GRE or SWI sequence is critical for accurate assessment of change, which is important in the setting of antibody based anti-amyloid immunotherapies which can have complications of amyloid related imaging abnormality (ARIA) [6].

Role of Structural Imaging in Neurodegeneration

It serves as a vital tool to rule out surgically amenable focal lesions such as tumors, hematoma, and vascular malformations. It also helps to differentiate AD from non-AD dementia by identifying patterns of gray-white matter atrophy which are best appreciated on 3D-T1WI. FLAIR is helpful in identifying white matter (WM) changes seen as chronic small vessel ischemia in vascular dementia (VD). Degree of vascular damage can be assessed on T2* GRE/SWI images where bleeds are seen as dark blooming foci. DWI and post-gadolinium images are crucial in the diagnostic workup of suspected rapidly progressive dementia with an infectious or inflammatory etiology. DWI is also helpful in excluding acute infarction in the setting of VD and hippocampal lesions in transient global amnesia [7]. ARIA in antibody treated AD individuals are seen as parenchymal edema or sulcal effusion on FLAIR and microbleeds or superficial siderosis on T2* GRE/SWI [6]. A stepwise approach can help narrow down the likely etiology of dementia (Fig. 11.1).

Degree of Atrophy

Visual assessment scales can be used to grade atrophy.

1. Global cortical atrophy scale (Pasquier scale): It is a 4-step scale that evaluates sulcal and ventricular dilation in various regions of the brain on T1 or FLAIR images. Graded as 0—normal/no ventricular enlargement, 1—opening of sulci/mild enlargement, 2—gyral atrophy/moderate enlargement, 3—"knife blade" gyral atrophy/severe enlargement [8].
2. ii. Medial temporal lobe atrophy scale (Scheltens' Scale): Based on width of choroid fissure & temporal horn, and height of hippocampal formation, atrophy can be assessed on a scale of 0–4 with very good sensitivity in senile-onset AD [9].

Loco-Regional Pattern of Atrophy

Loco-regional pattern analysis can help determine the type of dementia in some cases (Table 11.1) [7].

These visual assessments for volume loss require expert training and are limited by inter-rater variability. Recent trends involve the use of more sensitive automated quantitative techniques that allow cross-sectional and longitudinal analyses of the volumetric data from which patterns of atrophy and its progression in dementia can be evaluated. The commonly used volumetric software tools work either by cortical thickness-based or tissue-based segmentation. NeuroQuant (https://www.cortechs.ai/products/neuroquant/, USA) [10], Neuroreader (https://brainreader.net/, Denmark) [11], and Siemens Brain Morphometry (https://www.siemens-healthineers.com/, Germany) are approved by the United States Food and Drug Administration. Freesurfer (https://surfer.nmr.mgh.harvard.edu/, USA) [12], Voxel-Based Morphometry (https://neuro-jena.

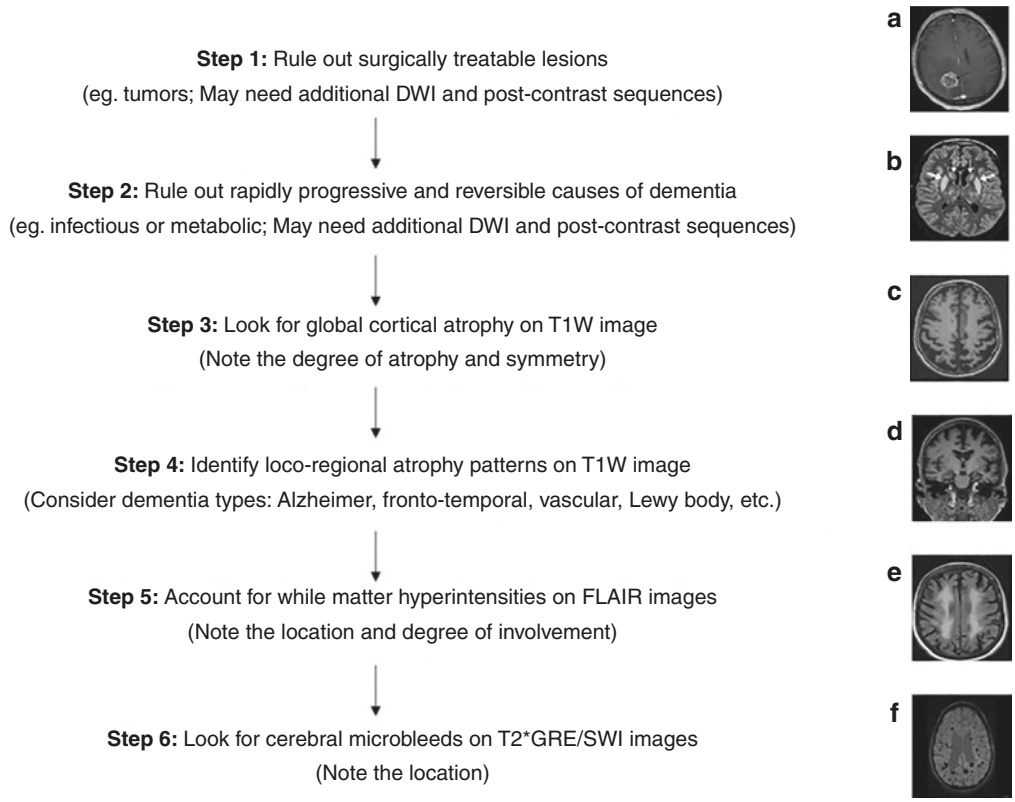

Fig. 11.1 Flowchart showing a stepwise approach to the diagnosis of dementia by imaging (DWI-diffusion weighted imaging, T1WI- T1 weighted imaging, FLAIR-fluid-attenuated inversion recovery, GRE- gradient recall echo, SWI- susceptibility weighted imaging). Data taken from [7]. (**a**) Coronal post-contrast image showing peripherally enhancing right temporal lobe tumor, (**b**) Axial DWI image showing restricted diffusion in bilateral cortices in Creutzfeldt-Jakob disease, (**c**) Axial T1W image showing bilateral parietal lobe atrophy, (**d**) Coronal T1W image showing bilateral temporal lobe atrophy, (**e**) Axial FLAIR image showing periventricular and deep white matter hyperintensities, (**f**) Axial T2*GRE image showing blooming foci in left temporal region representing microhemorrhages

Table 11.1 Loco-regional atrophy patterns and possible dementia subtypes. Data taken and modified from [7]

Location/pattern of atrophy	Possible dementia subtype
Hippocampus and/or medial temporal lobe	Usually AD (Fig. 11.2a), FTLD (Fig. 11.3c)
Posterior cingulate sulci and precuneus	Pre-senile AD (Fig. 11.2b, c)
Parietal lobes	Posterior cortical atrophy, usually AD (Fig. 11.2b, c)
Occipital lobes	Posterior cortical atrophy, mostly AD, dementia with Lewy bodies
Frontal and/or temporal lobes	FTLD (Fig. 11.3a, b) (right predominant-behavioral variant, left predominant- semantic variant)
Ventriculomegaly with disproportionate changes in subarachnoid spaces	Normal pressure hydrocephalus
Midbrain	Posterior supranuclear palsy
Pons with cerebellum	Multiple system atrophy
Cerebellum	Creutzfeldt-Jakob disease

AD Alzheimer's disease, *FTLD* frontotemporal lobar degeneration

github.io/software.html#vbm, Germany) [13] and FSL (https://fsl.fmrib.ox.ac.uk/fsl/fslwiki/, UK) [14] are used widely in research setting. The FreeSurfer quantified volumes can be plotted on individual longitudinal participant graphs comparing the results to a normative database [15] (Fig. 11.2d–f and 11.3d–h).

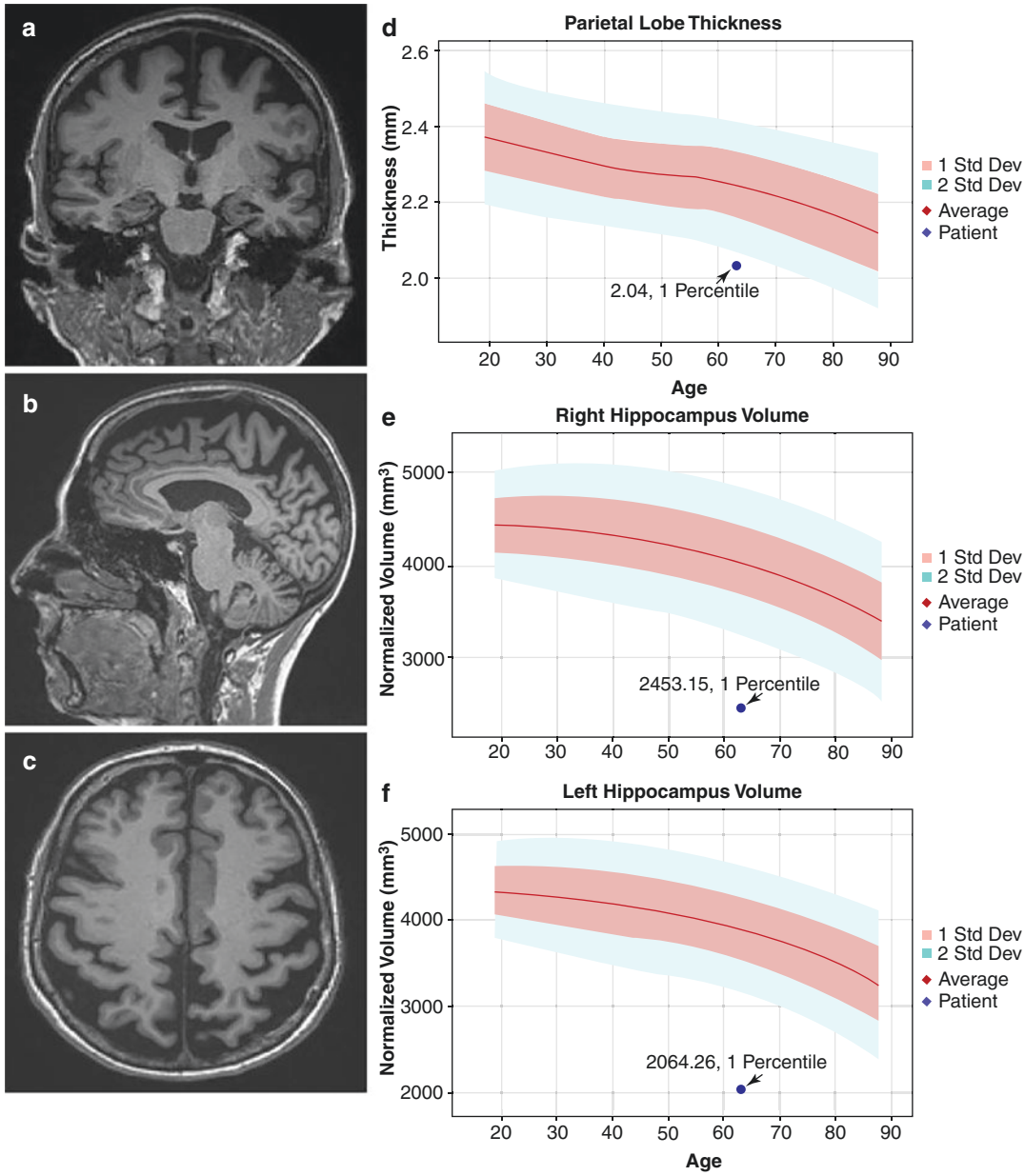

Fig. 11.2 MRI of 63-year-old white female with Alzheimer's dementia. (**a**) Coronal T1-WI showing bilateral hippocampal and temporal lobe atrophy (L > R) with Sylvian fissure widening. (**b**, **c**) Sagittal and axial sections of T1WI, respectively, showing gyral atrophy in parietal lobes including the precuneus with regional sulcal widening. Atrophy appears fairly symmetrical in either hemisphere with antero-posterior gradient. (**d**–**f**) Individual longitudinal participant (ILP) graphs showing FreeSurfer quantified volumes for parietal lobes and hippocampi at first percentile (< 2SD) compared to a normal database. (Image courtesy: Dr. Farzaneh Rahmani, Department of Radiology, Washington University in St. Louis)

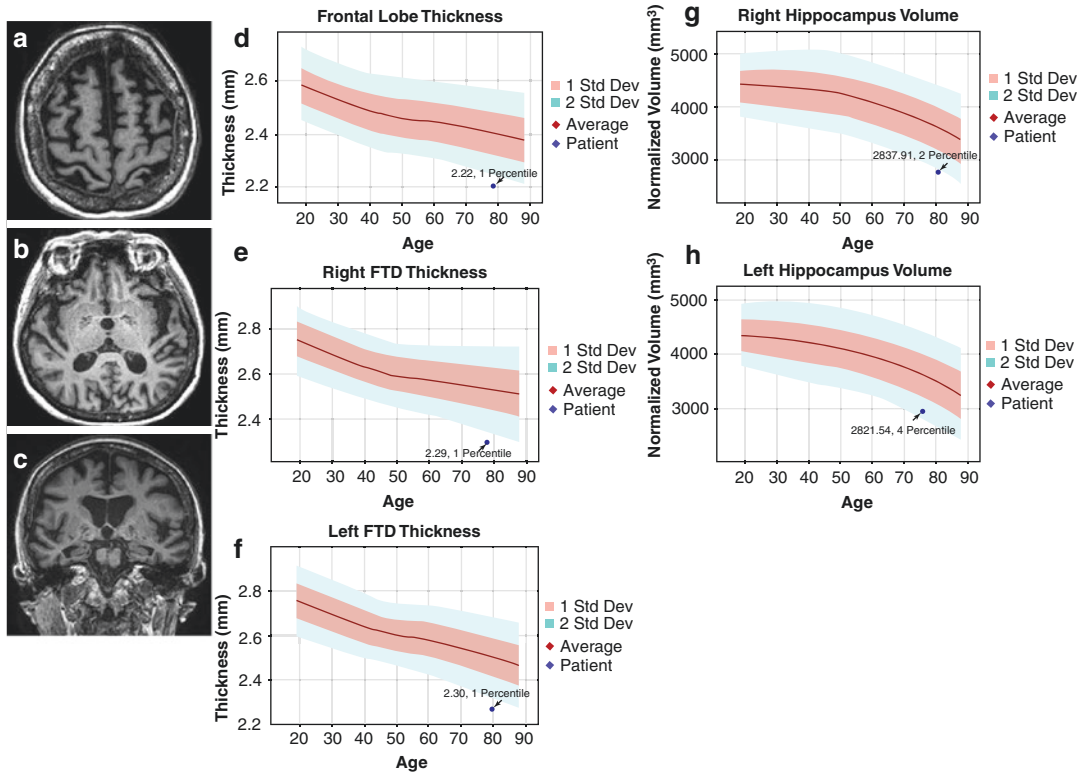

Fig. 11.3 MRI of 78-year-old white female with Frontotemporal lobar degeneration. (**a, b**) Axial sections of T1WI images showing gyral atrophy in bilateral frontal and temporal lobes, respectively, with regional sulcal widening. Atrophy appears slightly asymmetrical (L > R) in either hemisphere with an antero-posterior gradient. (**c**) Coronal T1-WI showing bilateral hippocampal and temporal lobe atrophy with Sylvian fissure widening. (**d–f**) Individual longitudinal participants (ILP) graphs showing FreeSurfer quantified volumes for frontal lobes and combined frontotemporal lobes at first percentile (< 2SD) when compared to a normal database. (**g, h**) ILP graphs showing FreeSurfer quantified volumes for right and left hippocampus at second and fourth percentile, respectively, when compared to a normal database. (Image courtesy: Dr. Farzaneh Rahmani, Department of Radiology, Washington University in St. Louis)

White Matter Hyperintensities (WMH)

WMH should be assessed for their location and degree of involvement. They can be periventricular, subcortical, and/or deep in location. Fazekas scoring is used to grade these changes in the periventricular and deep WM (Table 11.2) [16].

Cerebral microbleeds and Siderosis

Brain hemorrhages, most commonly consisting of cerebral microbleeds and/or superficial siderosis, are found in about 20% and 60% of patients with AD and VD, respectively, while seen only in 10% of the aging population [7]. They are also important component of ARIA in the setting of anti-amyloid immunotherapy [6]. Microbleeds are defined as 2–10 mm round hypointensities on T2*GRE/SWI images. They are better appreciated on SWI due to greater susceptibility and higher resolution. Lobar microhemorrhages are frequently seen with cerebral amyloid angiopathy, whereas central (basal ganglia, thalamus, and brainstem) microhemorrhages are more common with hypertensive encephalopathy. Superficial siderosis represents hemosiderin deposition along the leptomeninges, seen on MRI as hypointense signal with blooming on T2*GRE/SWI images.

Table 11.2 Fazekas scoring system. Data taken from [16]

Score	Periventricular WMH	Deep WMH	Inference
0	Absent	Absent	Normal
1	Caps	Punctate foci	Normal before 65 years
2	Smooth halo	Early confluence	Abnormal before 70 years
3	Irregular and extending to deep white matter	Large confluent areas	Always abnormal with poor cognitive outcomes

WMH white matter hyperintensities

Diffusion MRI Techniques

Diffusion MRI is an advanced imaging tool based on the property of diffusion of water molecules within the tissue at micron level. It assesses the integrity of axonal WM tracts along with their density and myelination characteristics. Imaging relies on fast diffusion encoding sequences such as echo-planar imaging (EPI). DTI and diffusion kurtosis imaging (DKI) are the commonly used diffusion techniques to assess the pathophysiology of neurodegenerative diseases [17].

Diffusion Tensor Imaging

DTI provides a quantitative evaluation of anisotropic diffusion of water molecules in the WM of brain using four metrics: fractional anisotropy (FA), mean diffusivity (MD), axial diffusivity, and radial diffusivity (RD). An increase in MD is seen in AD individuals due to disruption of cellular membrane impeding diffusion of water molecules. An abnormally decreased fractional anisotropy is also seen in AD due to loss of tract integrity [17]. DTI is also used in the diagnosis of Parkinson disease, amyotrophic lateral sclerosis, and traumatic brain injury (Table 11.3).

Limitations: (1) DTI is unable to detect GM changes as there is no information on the non-Gaussian diffusion of water molecules. (2) Presence of CSF and single compartment approximation results in a partial volume effect at the gray-white matter junction.

Table 11.3 Summary of the diffusion MRI findings in AD and PD. Data taken from [17–21]

Diffusion technique		AD	PD
DTI	MD	↑	↑
	FA	↓	↓
	Affected regions	Cingulate gyrus, precuneus, temporal lobe	Substantia nigra, frontal lobe, temporal lobe
	Special note	Volumetric MRI is superior for medial temporal lobe atrophy in early AD	DTI is not considered as diagnostic in early PD
DKI	MK	↓	↓
	AK	↓	–
	RK	↓	–
	Affected regions	White matter in the genu of corpus callosum, cingulum, temporal, frontal, and occipital regions	Substantia nigra, red nuclei, and anterior cingulum
	Special note	Changes in MK and AK have shown correlation with MMSE scores in occipital lobes	Together with QSM has a diagnostic accuracy of ~80–100%

AD Alzheimer disease, *PD* Parkinson disease, *DTI* diffusion tensor imaging, *MD* mean diffusivity, *FA* fractional anisotropy, *DKI* diffusion kurtosis imaging, *MK* mean kurtosis, *AK* axial kurtosis, *RK* radial kurtosis, *MMSE* mini-mental status examination, *QSM* quantity susceptibility mapping

Diffusion Kurtosis Imaging

DKI is useful in assessing GM by measuring the non-gaussian distribution of water molecules at the voxel level. A higher value of diffusion kurtosis corresponds with the deviation of water molecules from the Gaussian distribution, suggesting a more restricted environment. The opposite of this happens in neuronal loss. DKI describes the brain metrics using mean kurtosis (MK), axial kurtosis (AK), and radial kurtosis (RK). It has a role in the diagnosis of AD and PD (Table 11.3). It has been shown that DKI metrics are less affected by WMH and are more sensitive than DTI metrics in AD [17].

Resting-State Functional MRI

Principle and Acquisition

Hemodynamic changes are induced by regional neuronal activity due to neurovascular coupling. These changes result in dilution of the deoxygenated hemoglobin which acts as an endogenous contrast resulting in T2* prolongation and an increase in T2* MRI signals. This signal change is known as blood oxygen level dependent (BOLD) effect. Individuals with dementia are likely to have difficulty performing demanding cognitive tasks as a part of task-based fMRI. rsfMRI overcomes this limitation by acquiring continuous BOLD contrast images at rest. Acquisition of rsfMRI requires EPI with a TR of 2–3 s for 150–300 EPI volumes taken over 5–10 min of scan time [22]. The principle of rsfMRI by Biswal [23] and the default mode network (DMN) by Raichle [24] provided strong research evidence for use of rsfMRI in the evaluation of dementia in clinical setting.

Data Analysis

The rsfMRI data can be analyzed through various software packages such as statistical parametric mapping (http://www.fil.ion.ucl.ac.uk/spm/doc/) and FSL (http://fsl.fmrib.ox.ac.uk/fsl/fslwiki/). Functional connectivity between two remote brain regions is reflected by interregional correlation between low frequency (0.08–0.1 Hz) fluctuations. Correlation can be tested by paired region of interest (ROI), seed-to-voxel functional connectivity analysis or independent component analysis (ICA) [22, 23]. Seed-to-voxel analysis is a model-based method and easily comprehensible. ICA is a model-free analysis that generates resting-state network (RSN) maps with their individual temporal signal variations. ICA can be used to filter the physiological noise from pulsations in CSF [22]. RSN analysis can be done at an individual or group level each having their own advantages and disadvantages [25].

Role in Dementia Diagnosis

Individuals with AD have shown decreased resting-state functional connectivity compared to controls using seed-based ROI analysis (Fig. 11.4). Seed-based analysis of rsfMRI in 510 AD cases performed by Brier et al. showed abnormal RSN connectivity [26]. Reduced functional connectivity has been shown between in posterior cingulate cortex and hippocampus using seed-based analysis and ICA in AD [27, 28]. Classification performance based on combined seed- and ICA-based analysis was 97% in AD vs. controls advocating the usefulness of rsfMRI in AD diagnosis [29]. Easy technique and low burden on patients and radiologists permit the use of rsfMRI in clinical practice [22].

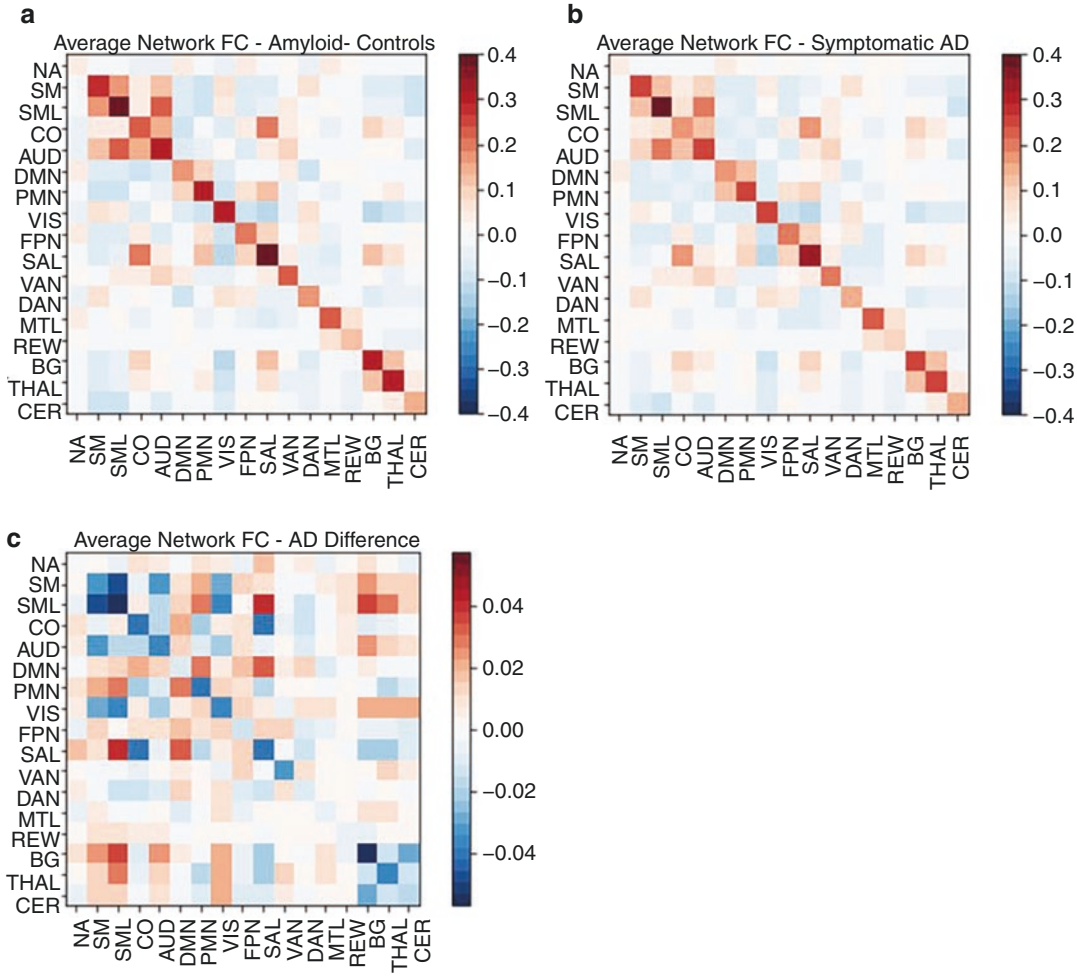

Fig. 11.4 AD-related differences in resting-state functional connectivity (RSFC). (**a**) Average RSFC within (along diagonal) and between networks (off diagonal) in amyloid-negative controls. (**b**) Average RSFC within and between networks in symptomatic AD participants. (**c**) Difference in RSFC between AD participants and controls. **Key**. For A and B, warm and cool colors indicate stronger positive and negative correlations, respectively. For C, cool colors indicate networks reduced connectivity in AD. *NA* unassigned regions, *SM* somatomotor network, *SML* lateral somatomotor network, *CO* cingulo-opercular network, *AUD* auditory network, *DMN* default mode network, *PMN* parietal memory network, *VIS* visual network, *FPN* fronto-parietal network, *SAL* salience network, *VAN* ventral attention network, *DAN* dorsal attention network, *MTL* medial temporal lobe network, *RE* reward network, *BG* basal ganglia network, *THAL* thalamus network, *CER* cerebellum network. ROIs and networks defined from Seitzman et al. [30]. (Image courtesy: Dr. Peter R. Millar, Department of Neurology, Washington University in St. Louis)

Magnetic Resonance Spectroscopy (MRS)

Principle and Acquisition

MRS is a noninvasive imaging tool to detect various metabolites and their concentrations in tissues based on the phenomenon of chemical shift imaging. Local magnetic field differences can produce a chemical shift due to changes in the resonance frequencies of the target nuclei (e.g., 1H). Results are plotted on a graph with chemical shift in ppm on x-axis and signal amplitude on y-axis. The area under the peak is proportional to the metabolite concentration. 1.5 T and 3 T scanners are able to show choline, creatine (Cr), glu-

tamine, myoinositol (mIns), and N-acetyle aspartate (NAA). Height of the peak changes with echo time (TE) which varies from 18 to 288 ms. Short TE has higher signal intensity and detects mIns. However, there is baseline distortion and peak superimposition at shorter TE leading to metabolite quantification errors. Volume localization in single-volume MRS can be obtained by stimulated echo acquisition mode and point-resolved spectroscopy [22].

Role of MR Spectroscopy in Dementia Diagnosis

A correlation between reduced NAA and senile plaques was shown by Klunk and colleagues [31]. Decrease in NAA or NAA/Cr by ~10–15% was seen in hippocampus, posterior cingulate, and precuneus in AD. These reductions are also seen in frontal lobe in frontotemporal lobar degeneration (FTLD), and occipital lobes in dementia with Lewy body [22]. Miller et al. demonstrated elevated mIns in addition to decreased NAA in the demented brain [32]. MRS alone is 64–94.1% sensitive and 72.7–92.3% specific in differentiating AD from healthy controls, while in conjunction with volumetric MRI sensitivity and specificity increases to 97% and 94%, respectively [33].

Caution is advised when interpreting metabolite derangements as age-related increase in Cr and decrease in NAA can be confounding factors. Metabolite changes on MRS can be observed before structural changes aiding in clinical diagnosis of dementia. In comparison to positron emission tomography, MRS can be done at the time of MRI examination making it fast and cost-effective. Concerns with acquisition parameters, quantitative assessment, and unavailability of standard values limit its clinical utility [22].

Arterial Spin Labeling MR Perfusion

Principle and Acquisition

Noninvasive MR perfusion imaging technique that uses inverted spins of arterial blood as an endogenous contrast. A perfusion-related signal is extracted by subtracting control images with normal spins from these labeled arterial blood images. 30–50 sets of these two sets of images have to be acquired over 4–5 min to increase SNR. 3 T MRI theoretically doubles the SNR compared to 1.5 T MRI although it increases the recovery time of inverted spins (1.6 s at 3 T vs. 1.4 s at 1.5 T). Acquisition of labeled images to quantify relative cerebral blood flow (rCBF) is delayed by 1.5–2 s for 3 T scanners to account for the arterial transit time (ATT). Patient motion and field inhomogeneity due to sinuses or implants could also interfere with rCBF [22].

Types

Pulsed ASL is easier to implement but has low SNR and higher sensitivity to ATT prolongation. Continuous ASL has a better signal in rCBF measurement due to longer labeling duration but also has a higher specific absorption rate. Pulsed-continuous ASL with short labeling pulses overcomes the disadvantage of higher absorption [22].

Role of ASL in Dementia Diagnosis

Although rCBF changes in dementia have been evaluated with single-photon emission computerized tomography (SPECT), ASL has higher spatial resolution and can be co-registered to a high-resolution 3D anatomical image overcoming partial volume effects in cortical GM voxels. Perfusion abnormalities seen with ASL in parietal lobes of AD individuals are consistent with changes seen on nuclear imaging studies [34, 35]. Efficacy of ASL in differentiating AD vs healthy subjects supports its clinical feasibility as a screening tool [36]. ASL is also useful in differentiating AD from FTLD by showing distinct areas of hypoperfusion [37].

Treatable and Reversible Dementias

Acute and treatable dementias have an atypical presentation. Prompt identification is critical for appropriate and effective treatment.

Infections

Sporadic Creutzfeldt-Jakob disease shows the areas of restricted diffusion on DWI images in thalamus (pulvinar sign), caudate, putamen, and cortex in the early stage of the disease with corresponding hyperintensities on T2/FLAIR images. Generalized brain atrophy with cortical thinning is evident in late stages. It should be differentiated from corticobasal degeneration which can present with myoclonus but shows caudate lobe and asymmetric premotor atrophy. **HIV-associated neurocognitive dysfunction/disorders** present with generalized brain atrophy, and T2/FLAIR subcortical and periventricular WMH without mass effect or enhancement. DTI reveals MD and FA abnormalities in the subcortical WM. **Progressive multifocal Leukoencephalopathy** is seen in immunocompromised patients (HIV or transplant recipients) as asymmetric multifocal T1 and T2 hyperintensities in the subcortical and periventricular WM along with U-fiber involvement. **Neuro-syphilis** is characterized by subcortical lesions in the temporal apex and insular gyri with meningeal enhancement, granulomas, and vasculitis-related basal ganglia infarctions [22].

Neoplasm

Lesions such as lymphomatosis cerebri and intravascular B-cell lymphomatosis can present with cognitive symptoms. Lymphomatosis cerebri appears as non-enhancing diffuse leukoencephalopathy on MRI. Intravascular B-cell lymphomatosis shows multifocal infarction-like findings inconsistent with regions of arterial supply and pontine hyperintensities that need differentiation from osmotic demyelination [22].

Chronic Subdural Hematoma (SDH)

AD mimicker and a known cause of reversible dementia especially, in elderly individuals. A meta-analysis of case-control studies showed traumatic brain injury as a risk factor for AD. It may exacerbate pre-existing dementia. Evacuation of the bleed has been shown to improve cognition and mental status in these patients [38].

Metabolic

Wernicke Encephalopathy occurs secondary to thiamine deficiency appearing as symmetrically enhancing T2/FLAIR hyperintensities in the thalamus, hypothalamus, and periaqueductal regions. **Hypoglycemic Encephalopathy** shows the areas of restricted diffusion in the corpus callosum, corona radiate, or internal capsule on DWI. Cortical and basal ganglia involvement denotes poor prognosis [22].

Post-Icteric Encephalopathy

It appears as T2/FLAIR hyperintensities and swelling of the cerebellum, hippocampus, amygdala, thalamus, and cortex with restricted diffusion on DWI Imaging plays an important role in differentiating it from encephalitis and metabolic encephalopathy thus prevent its progression to epilepsy [22].

Recent Advances in Imaging of Neurodegeneration

7T MRI

Ultrahigh-resolution MRI with ability to detect hippocampus atrophy at subfield level in mild cognitive impairment. Increased sensitiveness to susceptibility changes allows detection of microbleeds and iron-dense amyloid plaques invisible on routine imaging [39]. It can differentiate AD from controls with a specificity of 94.4% taking ≥5 microinfarcts as a cutoff [40].

Quantitative Susceptibility Mapping (QSM)

Iron is present in Aβ plaques and neurofibrillary tangles. QSM is based on multi-echo 3D GRE images and can help quantify iron overload

associated with AD, PD, and VD. A systemic review by Ravanfar and colleagues reported increased susceptibility changes or iron deposition in amygdala and dorsal striatum of AD subjects and in substantia nigra of PD individuals [41].

Neuroinflammation Imaging (NII) Using Diffusion

NII is an in vivo MR diffusion-based imaging technique developed to clinically image and quantify WM inflammation and damage in AD. Increased NII-derived cellular diffusivity was seen in both preclinical and early symptomatic phases of AD while decreased FA and increased RD indicating WM damage was only appreciated in symptomatic AD [42].

Quantitative Gradient Recalled Echo (qGRE) MRI

Identifies dark matter as a new imaging biomarker of neurodegeneration that precedes tissue atrophy in early AD. Kothapalli et al. used qGRE R2t* to identify hippocampal subfields with very low neuronal content (dark matter) and relatively preserved neurons (viable tissue). Compared to morphometric MRI, more significant differentiation was found between dark matter and viable tissue volume measurements between mild AD and controls [43].

Magnetization Transfer Imaging

It is based on the exchange of magnetization between macromolecules bound protons and free protons. By using off-resonance pulses and improving the image contrast it helps to provide information at the microstructural level. Colonna et al. found decreased magnetization transfer ratios in cortical, subcortical, and WM regions in AD individuals [44].

Summary

Brain MRI is an important tool for differential diagnosis and monitoring of neurodegenerative disorders and monitoring of therapy-related adverse events. Awareness of the applications of advanced structural and functional imaging biomarkers is essential for optimization of dementia imaging protocols.

Further Reading

For further overview and detailed explanations of imaging in various dementia subtypes and advanced MRI techniques refer to textbooks [7] and [22].

Acknowledgements Dr. Farzaneh Rahmani, M.D., Department of Radiology, Washington University in St. Louis.

Dr. Peter R. Millar, Ph.D., Department of Neurology, Washington University in St. Louis.

Grants NIH/NIA P50AG005681
NIH/NIA P01AG026276.
NIH/NIA P01AG003991.

References

1. Prince M, Bryce R, Albanese E, Wimo A, Ribeiro W, Ferri CP. The global prevalence of dementia: a systematic review and meta analysis. Alzheimers Dement. 2013;9(1):63–75.e2. https://doi.org/10.1016/j.jalz.2012.11.007.
2. McKhann GM, Knopman DS, Chertkow H, et al. The diagnosis of dementia due to Alzheimer's disease: recommendations from the National Institute on Aging-Alzheimer's Association workgroups on diagnostic guidelines for Alzheimer's disease. Alzheimers Dement. 2011;7(3):263–9. https://doi.org/10.1016/j.jalz.2011.03.005.
3. Park M, Moon WJ. Structural MR imaging in the diagnosis of Alzheimer's disease and other neurodegenerative dementia: current imaging approach and future perspectives. Korean J Radiol. 2016;17(6):827–45. https://doi.org/10.3348/kjr.2016.17.6.827.
4. Accreditation Support [Internet]. MRI exam-specific parameters: head and neck module. 2022. https://accreditationsupport.acr.org/support/solutions/articles/11000061019-mri-exam-specific-parameters-

head-and-neck-module-revised-4-6-2022-. Accessed 4 June 2022.
5. Jack CR Jr, Bernstein MA, Fox NC, et al. The Alzheimer's disease neuroimaging initiative (ADNI): MRI methods. J Magn Reson Imaging. 2008;27(4):685–91. https://doi.org/10.1002/jmri.21049.
6. Sperling RA, Jack CR Jr, Black SE, et al. Amyloid-related imaging abnormalities in amyloid-modifying therapeutic trials: recommendations from the Alzheimer's Association research roundtable workgroup. Alzheimers Dement. 2011;7(4):367–85. https://doi.org/10.1016/j.jalz.2011.05.2351.
7. Barkhof F, Fox NC, Bastos-Leite AJ, Scheltens P. Neuroimaging in dementia. Berlin: Springer; 2011.
8. Pasquier F, Leys D, Weerts JG, Mounier-Vehier F, Barkhof F, Scheltens P. Inter- and intraobserver reproducibility of cerebral atrophy assessment on MRI scans with hemispheric infarcts. Eur Neurol. 1996;36(5):268–72. https://doi.org/10.1159/000117270.
9. Scheltens P, Launer LJ, Barkhof F, Weinstein HC, van Gool WA. Visual assessment of medial temporal lobe atrophy on magnetic resonance imaging: interobserver reliability. J Neurol. 1995;242(9):557–60. https://doi.org/10.1007/BF00868807.
10. Brewer JB. Fully-automated volumetric MRI with normative ranges: translation to clinical practice. Behav Neurol. 2009;21(1):21–8. https://doi.org/10.3233/BEN-2009-0226.
11. Ahdidan J, Raji CA, DeYoe EA, et al. Quantitative neuroimaging software for clinical assessment of hippocampal volumes on MR imaging. J Alzheimers Dis. 2016;49(3):723–32. https://doi.org/10.3233/JAD-150559.
12. Dale AM, Fischl B, Sereno MI. Cortical surface-based analysis. I segmentation and surface reconstruction. Neuroimage. 1999;9(2):179–94. https://doi.org/10.1006/nimg.1998.0395.
13. Ashburner J, Friston KJ. Voxel-based morphometry—the methods. NeuroImage. 2000;11(6 Pt 1):805–21. https://doi.org/10.1006/nimg.2000.0582.
14. Jenkinson M, Beckmann C, Behrens TEJ, Woolrich MW, Smith SM. FSL. NeuroImage. 2012;62(2):782–90. https://doi.org/10.1016/j.neuroimage.2011.09.015.
15. Koenig LN, Day GS, Salter A, et al. Select atrophied regions in Alzheimer disease (SARA): an improved volumetric model for identifying Alzheimer disease dementia. Neuroimage Clin. 2020;26:102248. https://doi.org/10.1016/j.nicl.2020.102248.
16. Fazekas F, Chawluk JB, Alavi A, Hurtig HI, Zimmerman RA. MR signal abnormalities at 1.5 T in Alzheimer's dementia and normal aging. AJR Am J Roentgenol. 1987;149(2):351–6. https://doi.org/10.2214/ajr.149.2.351.
17. Kamagata K, Andica C, Kato A, et al. Diffusion magnetic resonance imaging-based biomarkers for neurodegenerative diseases. Int J Mol Sci. 2021;22(10):5216. Published 2021 May 14. https://doi.org/10.3390/ijms22105216.
18. Teipel SJ, Wegrzyn M, Meindl T, et al. Anatomical MRI and DTI in the diagnosis of Alzheimer's disease: a European multicenter study. J Alzheimers Dis. 2012;31(Suppl 3):S33–47. https://doi.org/10.3233/JAD-2012-112118.
19. Atkinson-Clement C, Pinto S, Eusebio A, Coulon O. Diffusion tensor imaging in Parkinson's disease: review and meta-analysis. Neuroimage Clin. 2017;16:98–110. https://doi.org/10.1016/j.nicl.2017.07.011. Published 2017 Jul 15.
20. Yuan L, Sun M, Chen Y, et al. Non-Gaussian diffusion alterations on diffusion kurtosis imaging in patients with early Alzheimer's disease. Neurosci Lett. 2016;616:11–8. https://doi.org/10.1016/j.neulet.2016.01.021.
21. Ito K, Ohtsuka C, Yoshioka K, et al. Differential diagnosis of parkinsonism by a combined use of diffusion kurtosis imaging and quantitative susceptibility mapping. Neuroradiology. 2017;59(8):759–69. https://doi.org/10.1007/s00234-017-1870-7.
22. Matsuda H, Asada T, Tokumaru AM, editors. Neuroimaging diagnosis for Alzheimer's disease and other dementias. Springer: Tokyo; 2017.
23. Biswal B, Yetkin FZ, Haughton VM, Hyde JS. Functional connectivity in the motor cortex of resting human brain using echo-planar MRI. Magn Reson Med. 1995;34(4):537–41. https://doi.org/10.1002/mrm.1910340409.
24. Raichle ME, MacLeod AM, Snyder AZ, Powers WJ, Gusnard DA, Shulman GL. A default mode of brain function. Proc Natl Acad Sci U S A. 2001;98(2):676–82. https://doi.org/10.1073/pnas.98.2.676.
25. Cole DM, Smith SM, Beckmann CF. Advances and pitfalls in the analysis and interpretation of resting-state FMRI data. Front Syst Neurosci. 2010;4:8. https://doi.org/10.3389/fnsys.2010.00008. Published 2010 Apr 6.
26. Brier MR, Thomas JB, Snyder AZ, et al. Loss of intranetwork and internetwork resting state functional connections with Alzheimer's disease progression. J Neurosci. 2012;32(26):8890–9. https://doi.org/10.1523/JNEUROSCI.5698-11.2012.
27. Zarei M, Beckmann CF, Binnewijzend MA, et al. Functional segmentation of the hippocampus in the healthy human brain and in Alzheimer's disease. NeuroImage. 2013;66:28–35. https://doi.org/10.1016/j.neuroimage.2012.10.071. [published correction appears in Neuroimage. 2013 Dec;83:1109].
28. Greicius MD, Srivastava G, Reiss AL, Menon V. Default-mode network activity distinguishes Alzheimer's disease from healthy aging: evidence from functional MRI. Proc Natl Acad Sci U S A. 2004;101(13):4637–42. https://doi.org/10.1073/pnas.0308627101.
29. Koch W, Teipel S, Mueller S, Benninghoff J, Wagner M, Bokde ALW, Hampel H, Coates U, Reiser M, Meindl T. Diagnostic power of default mode network

resting state fMRI in the detection of Alzheimer's disease. Neurobiol Aging. 2012;33(3):466–78. https://doi.org/10.1016/j.neurobiolaging.2010.04.013.
30. Seitzman BA, Gratton C, Marek S, et al. A set of functionally-defined brain regions with improved representation of the subcortex and cerebellum. NeuroImage. 2020;206:116290. https://doi.org/10.1016/j.neuroimage.2019.116290.
31. Klunk WE, Panchalingam K, Moossy J, McClure RJ, Pettegrew JW. N-acetyl-L-aspartate and other amino acid metabolites in Alzheimer's disease brain: a preliminary proton nuclear magnetic resonance study. Neurology. 1992;42(8):1578–85. https://doi.org/10.1212/wnl.42.8.1578.
32. Miller BL, Moats RA, Shonk T, Ernst T, Woolley S, Ross BD. Alzheimer disease: depiction of increased cerebral myo-inositol with proton MR spectroscopy. Radiology. 1993;187(2):433–7. https://doi.org/10.1148/radiology.187.2.8475286.
33. Westman E, Wahlund LO, Foy C, et al. Combining MRI and MRS to distinguish between Alzheimer's disease and healthy controls. J Alzheimers Dis. 2010;22(1):171–81. https://doi.org/10.3233/JAD-2010-100168.
34. Binnewijzend MA, Kuijer JP, Benedictus MR, et al. Cerebral blood flow measured with 3D pseudocontinuous arterial spin-labeling MR imaging in Alzheimer disease and mild cognitive impairment: a marker for disease severity. Radiology. 2013;267(1):221–30. https://doi.org/10.1148/radiol.12120928.
35. Musiek ES, Chen Y, Korczykowski M, et al. Direct comparison of fluorodeoxyglucose positron emission tomography and arterial spin labeling magnetic resonance imaging in Alzheimer's disease. Alzheimers Dement. 2012;8(1):51–9. https://doi.org/10.1016/j.jalz.2011.06.003.
36. Mak HK, Qian W, Ng KS, et al. Combination of MRI hippocampal volumetry and arterial spin labeling MR perfusion at 3-tesla improves the efficacy in discriminating Alzheimer's disease from cognitively normal elderly adults. J Alzheimers Dis. 2014;41(3):749–58. https://doi.org/10.3233/JAD-131868.
37. Hu WT, Wang Z, Lee VM, Trojanowski JQ, Detre JA, Grossman M. Distinct cerebral perfusion patterns in FTLD and AD. Neurology. 2010;75(10):881–8. https://doi.org/10.1212/WNL.0b013e3181f11e35.
38. Sahyouni R, Goshtasbi K, Mahmoodi A, Tran DK, Chen JW. Chronic subdural hematoma: a perspective on subdural membranes and dementia. World Neurosurg. 2017;108:954–8. https://doi.org/10.1016/j.wneu.2017.09.063.
39. McKiernan EF, O'Brien JT. 7T MRI for neurodegenerative dementias in vivo: a systematic review of the literature. J Neurol Neurosurg Psychiatry. 2017;88(7):564–74. https://doi.org/10.1136/jnnp-2016-315022.
40. van Rooden S, Goos JD, van Opstal AM, et al. Increased number of microinfarcts in Alzheimer disease at 7-T MR imaging. Radiology. 2014;270(1):205–11. https://doi.org/10.1148/radiol.13130743.
41. Ravanfar P, Loi SM, Syeda WT, et al. Systematic review: quantitative susceptibility mapping (QSM) of brain iron profile in neurodegenerative diseases. Front Neurosci. 2021;15:618435. https://doi.org/10.3389/fnins.2021.618435. Published 2021 Feb 18.
42. Wang Q, Wang Y, Liu J, et al. Quantification of white matter cellularity and damage in preclinical and early symptomatic Alzheimer's disease. Neuroimage Clin. 2019;22:101767. https://doi.org/10.1016/j.nicl.2019.101767.
43. Kothapalli SVVN, Benzinger TL, Aschenbrenner AJ, et al. Quantitative gradient Echo MRI identifies dark matter as a new imaging biomarker of neurodegeneration that precedes tissue atrophy in early Alzheimer's disease. J Alzheimers Dis. 2022;85(2):905–24. https://doi.org/10.3233/JAD-210503.
44. Colonna I, Koini M, Pirpamer L, et al. Microstructural tissue changes in Alzheimer disease brains: insights from magnetization transfer imaging. AJNR Am J Neuroradiol. 2021;42(4):688–93. https://doi.org/10.3174/ajnr.A6975.